rate of a ground-state two-photon transition in the ν_3 mode of SF_6. In so much as one can ignore multilevel effects that could produce inhomogeneous dephasing, this rate relates directly to the intramolecular dephasing rate for this level and is in good agreement with numerical calculations.

The authors would like to express their appreciation to J. Ackerhalt and A. Galbraith for helpful discussions and to O. P. Judd for discussions concerning alternative interpretations.

This work was supported in part by the U.S. Department of Energy under Contract No. ED-78-C-08-1563.

[1]L. S. Vasilenko, V. P. Chebotayev, and A. V. Shishaev, Pis'ma Zh. Eksp. Teor. Fiz. 12, 161 (1970) [JETP Lett. 12, 113 (1970)]; V. S. Letokhov and V. P. Chebotayev, *Nonlinear Laser Spectroscopy* (Springer, Berlin, 1977).

[2]A. H. Zewail, T. E. Orlowski, K. E. Jones, and D. E. Godar, Chem. Phys. Lett. 48, 256 (1977).

[3]M. M. T. Loy, in *Laser Spectroscopy* III, edited by J. L. Hall and J. L. Carlsten (Springer, Berlin, 1977), p. 435.

[4]H. S. Kwok and E. Yablonovitch, in *Picosecond Phenomena*, edited by C. V. Shank, E. P. Ippen, and S. L. Shapiro (Springer, Berlin, 1978), p. 218; D. S. Frankel, J. Chem. Phys. 65, 1696 (1976).

[5]T. Mossberg, A. Flusberg, T. Kachru, and S. R. Hartmann, Phys. Rev. Lett. 39, 1523 (1978).

[6]P. F. Liao, N. P. Economou, and R. R. Freeman, Phys. Rev. Lett. 39, 1473 (1977).

[7]For a recent review see A. Yariv, IEEE J. Quantum Electron. 14, 650 (1978).

[8]R. C. Lind, D. G. Steel, M. B. Klein, R. L. Abrams, C. R. Giuliano, and R. K. Jain, Appl. Phys. Lett. 34, 457 (1979).

[9]R. L. Abrams and R. C. Lind, Opt. Lett. 2, 94 (1978), and 3, 235 (1978).

[10]D. G. Steel, R. C. Lind, J. F. Lam, and C. R. Giuliano, Appl. Phys. Lett. 35, 376 (1979).

[11]D. M. Larsen and N. Bloembergen, Opt. Commun. 17, 254 (1976).

[12]A convenient tabulation of relevant SF_6 parameters is given by R. V. Ambartzumian and V. S. Letokhov, in *Chemical and Biochemical Applications of Lasers*, edited by C. Bradley Moore (Academic, New York, 1977), Vol. 3, p. 167.

[13]M. F. Goodman, J. Stone, and D. Dows, J. Chem. Phys. 65, 5052 (1976).

[14]A review of the semiclassical results is presented by N. Bloembergen, *Nonlinear Optics* (Benjamin, Reading, Mass., 1965), p. 21.

[15]H. W. Galbraith and J. R. Ackerhalt, private communication.

[16]J. R. Ackerhalt and H. W. Galbraith, J. Chem. Phys. 69, 1200 (1978).

Saturation of Brillouin Backscatter

Mark J. Herbst, Christopher E. Clayton, and Francis F. Chen
University of California, Los Angeles, California 90024

(Received 15 August 1979)

Saturation of Brillouin backscatter is observed from underdense plasma targets with CO_2 laser intensities as low as 2×10^{11} W/cm^2. Maximum reflectivity is about 5%, implying an ion-wave amplitude of 1%. The most likely limiting mechanism is found to be ion trapping, which is effective at our low T_e/T_i ratio.

Light loss due to reflective instabilities continues to be the most worrisome plasma effect in laser-driven fusion. In solid-target experiments, energy reflectivities attributed to stimulated Brillouin scattering (SBS) have varied from 0 to 50% for glass lasers[1-6] and 1 to 30% for iodine lasers,[7] and are close to 5% for CO_2 lasers.[8-10] Widely varying conditions and the complications of critical layers and plasma flow make it difficult to specify the saturation mechanism. Experiments using underdense plasma targets have also given divergent results ranging from 1% (Ref. 11) to 60% (Ref. 12). In our work, a Brillouin reflectivity[13] of $\simeq$5% is measured and is explained by ion trapping. Because of ionization-front effects discovered to be operative in such experiments,[14] particular care was taken to verify the Brillouin nature of the backscatter.

We used a 30-J CO_2-laser system producing 300-MW pulses with 50 nsec full width at half maximum (FWHM), followed by $a \simeq 1$-μsec tail of $\simeq$30-MW average power. The 10-cm-diam annular beam is focused to 280 ± 30 μm FWHM by an $f/7.5$ Ge lens. The plasma target is an arc discharge in 15.2 Torr of H_2, 2.5 cm in diameter, partially ionized to $n = 10^{16}$ cm^{-3} and $T_i \simeq T_e = 4$–5

eV. The CO_2-laser beam is incident radially and focused at the center of the cylindrical plasma, creating a cigar-shaped, laser-heated, fully ionized interaction region, whose properties are documented by visible spectroscopy and ruby interferometry.[14]

Timing of incident and reflected signals from Mylar beam splitters and nanosecond photon-drag detectors is shown in Fig. 1. Backscatter is seen to occur in short spikes 10–30 nsec after peak incident power. Spectra are taken with shot-to-shot scanning of a Fabry-Perot interferometer, using Cu:Ge and Hg:Ge photodetectors at 4 °K. Figure 2 shows a backscatter spectrum having a typical redshift of 23 GHz. To reduce statistical fluctuations the data are normalized to total backscatter on each shot, as obtained on the second detector.

This redshift eliminates the possibility of Raman scattering ($\Delta f \simeq -4000$ GHz) or of stray light induced by refraction. Besides SBS, this redshift could also be caused by reflection at the dielectric discontinuity of a moving, laser-supported ionization wave.[15] To eliminate this mechanism, two further tests are made. First, ray retracing [a characteristic of SBS (Ref. 2)] is checked by masking half the incident beam. It is found that rays do retrace, with > 90% of the backscattered light going back into the unmasked half. Second, dielectric reflection is purposely induced by raising the pressure to 150 Torr, above the laser breakdown threshold. Reflected signals then have a completely different signature: Pulse shape mirrors the incident pulse; spectra are blue shifted (from an ionization front moving toward the lens); and rays do not retrace.

Having identified true SBS signals, we next used attenuators to study how they saturate. Figure 3 shows peak reflectivity versus input power up to 300 MW, which, if one neglects self-focusing, would correspond to $I_0 \simeq 5\times10^{11}$ W/cm^2. The reflectivity R first grows rapidly with I_0, then saturates at $\simeq 5\%$. We analyze these two regions in turn.

In the growth region, our conditions are best fitted by the theory of convective instabilities in a finite, homogeneous plasma. Ion-density fluctuations are driven up by the beat between the incoming (ω_0, k) and backscattered (ω_2, k_2) light waves; the backscattered wave, in turn, is created by Bragg scattering off the ion wave (ω_i, k_i). Since T_e/T_i is small (<10), the ion waves are heavily Landau damped and will grow to an amplitude where their energy loss is balanced by input from the pump. In this case both the ion wave and the scattered power P_s depend exponentially[16] on I_0:

$$P_s = P_n \exp[2\,\mathrm{Im}(k)L], \tag{1}$$

where L is the interaction length, P_n is the scattering from the initial level of ion fluctuations, and[17]

$$\mathrm{Im}(k) = \frac{k_0 v_0^2}{2c^2}\,\mathrm{Im}\left(\frac{\chi_e(1+\chi_i)}{1+\chi_e+\chi_i}\right). \tag{2}$$

Here χ_e and χ_i are the electron and ion susceptibilities at (ω_i, k_i) and v_0 is the peak electron quiver velocity ($\propto I_0^{1/2}$) in the pump field. We have omitted writing the negligible damping and dispersion of the light waves in the underdense plasma. When χ_e and χ_i are expanded in small

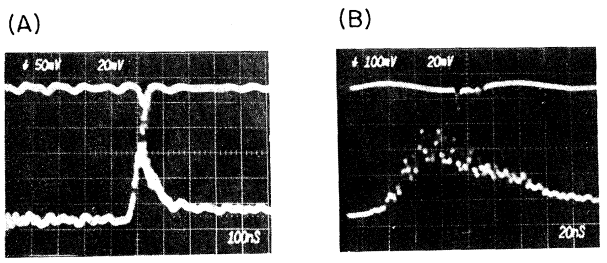

FIG. 1. Relative timing of pump (bottom traces) and backscatter (top traces) signals on (a) 100-nsec/div and (b) 20-nsec/div sweeps.

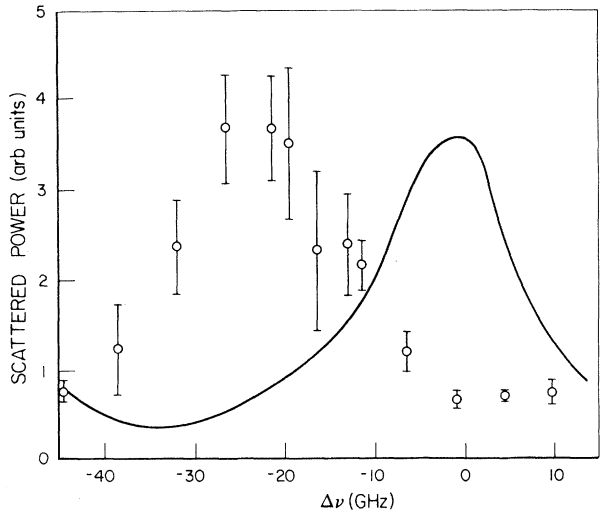

FIG. 2. Spectra of backscatter (points) and incident light (curve), showing redshift. Each point is an average of five shots.

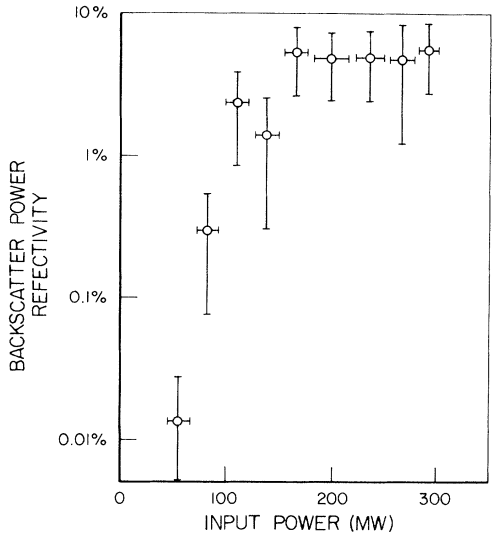

FIG. 3. Reflectivity vs pump power, showing saturation. Reflectivity is defined as peak power back into input optics divided by input power at that time.

T_i/T_e and $k_i^2\lambda_D^2$, one obtains the familiar result[16]

$$P_s = P_n \exp(2\gamma_0^2 L/c\gamma_i), \tag{3}$$

where γ_0 is the SBS growth rate in an infinite, homogeneous plasma and γ_i is the ion-wave damping rate. In practice, T_e/T_i as small as 2 is covered by using a γ_i and an ω_i consistent with Eq. (2).

The growth region of Fig. 3 can be fitted to the exponential of Eq. (3) if n_e (which enters in γ_0^2), T_e/T_i (which enters in γ_i), and L do not vary with I_0. Our backscatter grows in a long, uniform region of hot, expanded plasma behind a dense, cold ionization front.[14] Holography shows that here n_e is approximately constant at $(1.5 \pm 0.5)\times 10^{17}$ cm^{-3} regardless of I_0. The redshift is measured to be independent of I_0, indicating constant T_e (for constant T_e/T_i), since $\omega_i = k_i c_s = k_i (KT_e/M + 3KT_i/M)^{1/2}$. The ratio T_e/T_i is determined by electron-ion equilibration and thus is constant if T_e is constant. Computations of the time-dependent transport problem,[18] as well as a simple dimensional argument,[19] show $T_e/T_i \simeq 3$. Using this, one infers from the redshift a value $T_e \simeq 80$ eV, corresponding to a maximum value of $v_0^2/v_e^2 = 0.25$ in this experiment. One then finds that Eq. (3) and the slope of Fig. 3 are consistent if $L = 10 \pm 4$ mm, which is half the length of uniform plasma seen holographically. L is apparently determined by focal depth and hence does not vary with I_0 either. Using $L = I_0^{-1} \int I(z)\,dz$, with $I(z)$ measured, we find $L = 8 \pm 1$ mm, in reasonable agreement with that found from the slope of the growth curve.[20]

If T_e, T_i, n_e, and L do not vary with I_0, one can extrapolate the curve of Fig. 3 to $I_0 = 0$ to obtain the initial noise level from which the backscattered wave grows. One then obtains $P_n \simeq (10^{-7}-10^{-5})P_0$, which is 10^3–10^5 times the thermal Thomson-scattering level. This enhancement factor agrees well with other experiments on shock-enhanced acoustic turbulence,[21,22] suggesting that the noise source for the SBS is ion turbulence at the ionization front.

We now consider the saturation region of Fig. 3. Suppose the peak ion wave amplitude $\tilde{n}/n$ is fixed (by ion trapping, say) over a length L. Then the expression for reflectivity including pump depletion[23] reduces for $R < 20\%$ to the usual Bragg scattering formula

$$R = (\tfrac{1}{2}\tilde{n}\lambda_0 L r_0)^2 = \left(\frac{\pi}{2}\frac{L}{\lambda_0}\frac{\tilde{n}}{n}\frac{n}{n_c}\right)^2, \tag{4}$$

where $r_0 = e^2/mc^2$. In our case, where $n/n_c = 0.015$, $L = 1$ cm, and $R = 5\%$, this gives $\tilde{n}/n = 1\%$. On the other hand, if $\tilde{n}/n$ grows from noise to a finite level within the interaction region L, the expression for reflectivity including pump depletion has been given.[4,23] For $R \simeq 5\%$, pump depletion is unimportant, and this expression reduces to Eq. (3). In this case, where ion damping balances parametric growth, $\tilde{n}/n$ is given by[23]

$$\frac{\tilde{n}}{n} = \frac{2\pi e^2}{mMc^3}\frac{k_i^2}{k_0^2}\frac{I_0 R^{1/2}}{\gamma_i \omega_i} \tag{5}$$

with I_0 in units of ergs/cm^2 sec. This formula holds up to the beginning of saturation, around $I_0 = 2.5\times 10^{11}$ W/cm^2. At this intensity, our parameters yield $\tilde{n}/n \simeq 2.4\%$, in good agreement with the 1% given by Eq. (4), which assumes $\tilde{n}$ constant in space and gives therefore an average $\tilde{n}$.

Since R does not increase with I_0 in the saturation region, $\tilde{n}$ must also be independent of I_0. This is just Bragg scattering from a fixed grating. Various mechanisms have been proposed for limiting the size of $\tilde{n}$: (1) pump depletion,[23-25] (2) wave breaking,[25-27] (3) energy and momentum deposition,[28] (4) electron heating,[29] (5) harmonic generation,[30] (6) ion trapping,[23] and (7) ion heating.[23] Effects (1)–(4) cannot account for our low ($\tilde{n}/n \simeq 1\%$) saturation level. Effect (5) is the steepening os sinusoidal waves into sawteeth and is supposed[30] to occur for $\tilde{n}/n = k^2\lambda_D^2$ ($\simeq 3\%$ in our case). This level is only slightly higher than ob-

served, but there has been no experimental verification of this theoretical prediction.

Ion trapping has been seen in computer simulations,[26] but only one analytic result for the saturation level exists[30]:

$$\tilde{n}/n \simeq \tfrac{1}{2}\{[1+(T_i/T_e)]^{1/2} - (3T_i/T_e)^{1/2}\}^2. \quad (6)$$

This result comes from a waterbag model in which $f_i(v)$ is flat up to $\pm 3^{1/2}v_i$. For $T_e/T_i = 3$, this predicts $\tilde{n}/n \simeq 1.2\%$, in good agreement with the value computed from Eq. (4) for $R = 5\%$. Here the trapping of ions in the bulk of the distribution clamps $\tilde{n}/n$ to a low value independent of I_0. The trapped ions can cause a nonlinear frequency shift, which has been computed and checked experimentally.[31] When this shift equals the half width at half maximum of the Brillouin growth versus frequency curve, as computed from Eq. (1), the expected[31] amplitude is $\tilde{n}/n \simeq 0.8\%$ at $T_e/T_i = 3$.

Ion heating causes saturation in a different way: T_i is increased by ion wave damping, and the decrease in T_e/T_i causes γ_i to increase, turning off the instability. Using the Manley-Rowe relation, we estimate that the maximum energy the ions could receive at the measured values of R and I_0 could change T_e/T_i only from 3 to 2.5 in the saturation region. The corresponding increase in γ_i is not enough to explain the constancy of $\tilde{n}/n$ for intensities above $I_0 = 2.5\times10^{11}$ W/cm^2. In our case, T_e/T_i is set by collisional processes in the evolution of the laser-heated region and cannot vary much during the backscatter pulse.

We have shown, therefore, that ion trapping is the most plausible mechanism for saturating R at 5% in our experiment. Because the level at which the ion waves saturate is set by T_e/T_i, comparable levels would be expected as a result of trapping in solid-target experiments where low values of T_e/T_i may also exist. This mechanism can limit the ion waves long before the other possible saturation mechanisms become important. If $\tilde{n}/n$ is clamped by trapping, reflectivity will scale according to Eq. (4).

Our conclusions depend on the absence of (a) three-dimensional effects at low f numbers, (b) any I_0 effect on P_n, and (c) self-focusing or filamentation. Existence of (c) would increase I_0 locally, thus driving $\tilde{n}$ to higher values; but then L would have to be smaller, according to Eq. (4), to explain the observed R. Though smaller L is likely with (c), saturation of R requires $\tilde{n}L$ to be fortuitously constant with I_0. No filamentation is expected[32] at our low values of T_e/T_i and $\mathrm{Im}(k)L$, and only whole-beam self-focusing is observed in studies of the transmitted CO_2-laser beam.[19] Interferometry[14] shows that self-focusing density profiles exist, but not where they affect I_0 in the SBS growth region.

We have benefitted from useful conversations with R. P. Godwin, W. L. Kruer, N. C. Luhmann, Jr., B. Ripin, and others. This work was supported by the U. S. Department of Energy, Contract No. EY-76-S-03-0034, P.A. 236; Los Alamos Scientific Laboratory, P.O. No. 4-X49-0027K1; and the National Science Foundation, Grants No. 75-16610 and No. 77-17861.

[1]L. M. Goldman, J. Soures, and M. J. Lubin, Phys. Rev. Lett. 31, 1184 (1973).
[2]B. H. Ripin *et al.*, Phys. Rev. Lett. 33, 634 (1974).
[3]B. H. Ripin *et al.*, Phys. Rev. Lett. 39, 611 (1977).
[4]D. W. Phillion, W. L. Kruer, and V. C. Rupert, Phys. Rev. Lett. 39, 1529 (1977).
[5]H. D. Shay *et al.*, Phys. Fluids 21, 1634 (1978).
[6]A. G. M. Maaswinkel, K. Eidmann, and R. Sigel, Phys. Rev. Lett. 42, 1625 (1979).
[7]K. Eidmann *et al.*, Max-Planck Institute, Garching, Germany, Report No. PLF-15, 1979 (unpublished).
[8]K. B. Mitchell, T. F. Stratton, and P. B. Weiss, Appl. Phys. Lett. 27, 11 (1975).
[9]V. Cottles and D. V. Giovanielli, Los Alamos Report No. LA-UR-77-1096, 1977 (unpublished).
[10]B. Grek, H. Pepin, and F. Rheault, Phys. Rev. Lett. 38, 898 (1977).
[11]D. W. Scudder, Ph.D. thesis, University of Washington, Seattle, Washington, 1979 (unpublished).
[12]A. Ng *et al.*, Phys. Rev. Lett. 42, 307 (1979).
[13]Peak reflected intensity in these long-pulse experiments is assumed to be indicative of time-integrated energy reflectivity in nanosecond experiments.
[14]M. J. Herbst, C. E. Clayton, and F. F. Chen, University of California, Los Angeles, Report No. UCLA PPG-424 (to be published).
[15]N. Ahmed, B. C. Gale, and M. H. Key, J. Phys. B 2, 403 (1969).
[16]D. W. Forslund, J. M. Kindel, and E. L. Lindman, Phys. Fluids 18, 1002 (1975).
[17]J. F. Drake *et al.*, Phys. Fluids 17, 778 (1974).
[18]J. J. Turechek and F. F. Chen (to be published).
[19]M. J. Herbst, University of California, Los Angeles, Report No. UCLA PPG-382, 1979 (unpublished).
[20]However, the latter is sensitive to T_e/T_i, which is not known accurately.
[21]M. Kornherr *et al.*, Phys. Lett. 39A, 95 (1972).
[22]N. L. Bretz and A. W. DeSilva, Phys. Rev. Lett. 32, 138 (1974).
[23]W. L. Kruer, Lawrence Livermore Laboratory Report No. UCRL-82701, 1979 (unpublished).
[24]D. W. Forslund, J. M. Kindel, and E. L. Lindman, Phys. Rev. Lett. 30, 739 (1973).

[25]W. L. Kruer, in *Advances in Plasma Physics*, edited by A. Simon and W. B. Thompson (Wiley, New York, 1976), Vol. 6, p. 237.
[26]D. W. Forslund, J. M. Kindel, and E. L. Lindman, Phys. Fluids 18, 1017 (1975).
[27]W. L. Kruer, Phys. Fluids 22, 1111 (1979).
[28]W. L. Kruer, E. J. Valeo, and K. G. Estabrook, Phys. Rev. Lett. 35, 1076 (1975).
[29]W. L. Kruer, K. G. Estabrook, and K. H. Sinz, Nucl. Fusion 13, 952 (1973).
[30]J. M. Dawson, W. L. Kruer, and B. Rosen, in *Dynamics of Ionized Gases*, edited by M. Lighthill, I. Imai, and H. Sato (Univ. of Tokyo Press, Tokyo, 1973), pp. 47–61.
[31]H. Ikezi *et al.*, Phys. Fluids 21, 239 (1978).
[32]R. H. Lehmberg, private communication.

Instantaneous Flux-Change Measurement of the Mobile Dislocation Density in Crystals

C. S. Pang[a] and J. M. Galligan
Department of Metallurgy and Institute of Materials Science, University of Connecticut, Storrs, Connecticut 06268
(Received 13 July 1979)

This Letter presents measurements of the mobile dislocation density in lead–5%-indium crystals, in which we measure the change in flux accompanying the motion of dislocations. In particular, it is shown that the present technique allows us to establish how the mobile dislocation density varies for crystals undergoing vastly different types of work hardening. In addition, we use the present technique to show how the mobile dislocation density varies with applied strain rate.

The plasticity of crystals occurs through the generation and motion of dislocations.[1] In addition, various microscopic theories of plasticity, which involve interactions among dislocations, explain the work hardening that accompanies plastic deformation in terms of particular average dependencies on the mobile dislocation density as a function of stress. This average mobile dislocation density, ρ_m, is either an adjustable parameter in theories of work hardening, or it is inferred from deformation experiments which measure the total dislocation density before and after deformation,[1] i.e., etch-pit studies, slip-line measurements, transmission electron microscopy. The variation of ρ_m with stress, strain, and applied strain rate is, in fact, central to any theory of work hardening, and has not been *instantaneously measured while a sample is deforming*. In the present paper, we show how a recently introduced technique can be used to measure the mobile dislocation density while the sample is deformed.[2]

The experiment relies on the fact that when a type-II superconductor, in the mixed state, is deformed the motion of the dislocations is accompanied by a change in flux. As such, then, the change in flux is a measure of the dislocations which are mobile, and in the present experiment we measure, through the change in flux of the mixed state of a superconductor, the variation of ρ_m as a function of stress, strain, and applied strain rate. In particular, results are presented on crystals which are oriented as follows: Crystals are oriented to deform initially, on a single-slip system. Such crystals exhibit three different work-hardening regions, one of which is a relatively low work-hardening rate while another work-hardening rate varies roughly as $G/300$, where G is the shear modulus of the crystal while the final work-hardening rate is variable and intermediate between the first and second.

The rapid work-hardening rate—$G/300$—has been the subject of a number of theoretical treatments of plasticity[3-5] as well as extensive experimental investigations. This particular work-hardening characteristic appears in almost all face-centered-cubic metals and alloys, as well as body-centered metals and some hexagonal metals.[1] As such, it is of interest to explain the presence of such a work-hardening rate, and experimental information on it is of importance. Furthermore, many metals and alloys which become superconductors do exhibit type-II behavior and lead-indium crystals have been used extensively in this regard.[6]

In order to carry out the present experiments, we have grown some lead–5%-indium single crystals, which are oriented for single slip and for multiple slip. Crystals of this composition exhibit typical type-II superconducting behavior. These crystals, grown by the standard Bridgman technique, prepared from 99.9999%-purity lead

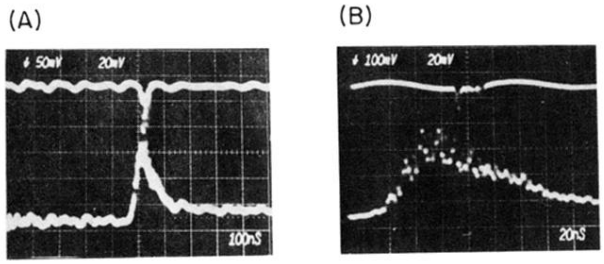

FIG. 1. Relative timing of pump (bottom traces) and backscatter (top traces) signals on (a) 100-nsec/div and (b) 20-nsec/div sweeps.